



Co/N-codoped porous carbons derived from poly(Schiff base)/Co(II) complex as ultrahighly efficient catalysts for CTH of nitroarenes

Weichao Xie^a, Bei Liu^a, Yijiang Liu^a, Hongbiao Chen^{a,**,*}, Mei Yang^a, Huaming Li^{a,b,*}

^a College of Chemistry, Xiangtan University, Xiangtan, 411105, Hunan Province, PR China

^b Key Laboratory of Polymeric Materials & Application Technology of Hunan Province, Key Laboratory of Advanced Functional Polymeric Materials of College of Hunan Province, and Key Laboratory of Environment-Friendly Chemistry and Application in Ministry of Education, Xiangtan University, Xiangtan, 411105, Hunan Province, PR China

ARTICLE INFO

Keywords:

Co/N-codoped porous carbons
Catalytic transfer hydrogenation
Poly(Schiff base)s
Nitroarenes
Chemoselectivity

ABSTRACT

Herein we report the scalable synthesis of Co/N-codoped porous carbon (Co/N-C) catalysts by pyrolyzing poly (Schiff base)/Co(II) complex. The strong Co(II)-binding affinity of poly(Schiff base) leads to the formation of uniformly distributed Co(0) nanoparticles, Co-N_x species, and N-C configurations, in which their catalytic contributions are confirmed and estimated by ligand-poisoning and acid-etching experiments and the Co-N_x species has been proved to be highly active for catalytic transfer hydrogenation (CTH) reaction. Consequently, the as-prepared Co-N/C-950 catalyst exhibits an ultrahigh activity for the CTH of 4-nitrophenol (4-NP) with a TOF of 226 mol_{4-NP} mol_{Co}⁻¹ min⁻¹ (13560 h⁻¹) together with an excellent selectivity for CTH of challenging nitroarenes. Moreover, the Co(0) nanoparticles embedded in the Co-N/C-950 catalyst can be further transformed to Co₄N phase by a facile nitridation reaction, yielding Co₄N-N/C-950 catalyst with even higher activity for the CTH of 4-NP (TOF up to 310 mol_{4-NP} mol_{Co}⁻¹ min⁻¹).

1. Introduction

Heterogeneous catalytic transfer hydrogenation (CTH) of nitroarenes is an effective and convenient approach to access aminoarenes because CTH reaction can proceed through hydrogen transfer from a hydrogen donor to nitroarenes with the assistance of catalysts [1–3]. In comparison with conventionally catalytic hydrogenation using flammable, pressurized H₂ gas, the use of hydrogen donors promise several advantages in terms of alleviating potential safety hazards, obviating the need for sophisticated equipments, and improving the solubility of hydrogen sources [4]. Moreover, most of the hydrogen donors, such as sodium borohydride [5], hydrazine [6], formic acid [7,8], and alcohol [9], etc., are inexpensive, water-soluble, and easy to handle in aqueous solution. Although CTH can date back to more than a century ago that was first proved by Knoevenagel in 1903 through Pd-promoted disproportionation reaction [10], only in recent years has CTH been widely used for the hydrogenation of nitroarenes. A variety of supported precious metal catalysts, such as Pd [11], Pt [12], Ru [13], and Rh [14], Au [15], etc., have therefore been synthesized and adopted to catalyze the CTH of nitroarenes, and some of which are even commercially available [16,

17]. However, the high-price and resource scarcity of such catalysts make them difficult to achieve large-scale application. For these reasons, the development of supported transition 3d-metal (Co, Fe, Ni, Cu, etc.) catalysts has attracted great interest due to the low-cost and abundant resources [18–21]. Among them, Co nanoparticles supported on N-doped carbon matrices (Co/N–C) have recently emerged as an important class of catalysts and received considerable attention [22–27]. At present, it is generally accepted that both carbon-encapsulated Co(0) nanoparticles and atomically dispersed Co-N_x species are the active sites in Co/N–C catalysts although the nature of the really active sites is still a matter of debate [23–25]. In addition, N-doping, especially N-bonding configurations, in carbon matrix plays an equally important role in promoting the activity and tuning the selectivity [26,27].

The use of Co-N/C catalysts in direct hydrogenation of nitroarenes was pioneered by Beller group in 2013, they prepared such catalysts by the solution impregnation of Co(II)/ligand complexes onto activated carbon (Vulcan XC72R) followed by pyrolysis [28]. Among the ligands examined (i.e., bis(2-benzimidazolyl)pyridine, terpyridine, bipyridine, pyridine, and phenanthroline), only phenanthroline-derived catalyst

* Corresponding author at: College of Chemistry, Xiangtan University, Xiangtan, 411105, Hunan Province, PR China.

** Corresponding author.

E-mail addresses: chenhongbiao@xtu.edu.cn (H. Chen), lihuaming@xtu.edu.cn (H. Li).

<https://doi.org/10.1016/j.apcata.2021.118249>

Received 23 March 2021; Received in revised form 10 May 2021; Accepted 6 June 2021

Available online 8 June 2021

0926-860X/© 2021 Elsevier B.V. All rights reserved.

(namely Co-Co₃O₄/NGr@C) can provide the best activity for the hydrogenation of nitroarenes with H₂ gas, revealing that the Co-N_x sites are vital to the catalytic activity. Shortly after that, such a Co-Co₃O₄/NGr@C catalyst was used to catalyze the CTH of nitroarenes by using formic acid as the hydrogen donor, in which excellent selectivity was proved by the unprecedented tolerance toward functional groups, such as olefins, ketone, aldehyde, nitrile, halides, ester, and amide [29]. Since then, much effort has been devoted to the preparation and utilization of the Co-N/C catalysts, in which the methods used to prepare these catalysts are basically the same, involving the pyrolysis of either carbon-supported/unsupported Co(II)/N-ligand complexes [30] or Co-salt/carbon-precursor mixture followed by nitrogenation [31]. Among these Co(II)/N-ligand complexes, the zeolite-type Co-imidazolate framework, namely ZIF-67, is one of the most commonly used precursor [32–36]. Li and co-workers reported, for the first time, the use of ZIF-67-derived Co-N/C catalyst in the CTH of nitroarenes [37]. Although the nitroarenes were hydrogenated to the corresponding aminoarenes with high chemoselectivity, the activity of Co-N/C catalyst remained to be improved due to the low BET specific surface area ($S_{\text{BET}} \approx 130 \text{ m}^2 \text{ g}^{-1}$), which would be adverse to the exposure of active sites as well as the mass transfer. Later on, the catalytic activity of ZIF-67-derived Co-N/C catalysts has been greatly enhanced through the use of hard templates (i.e., SiO₂ [34], SBA-15 [38], graphene oxide [39], carbon nanotubes [40], etc.) and bimetallic ZIF precursors [41], or through the pre-treatment of ZIF-67 with heteroatom-enriched organic molecules (i.e., urea, thioacetamide) [42,43] and polymers [44,45]. In these ways, the Co-N/C catalysts can be engineered to have high S_{BET} and/or to possess highly dispersed active sites (i.e., Co-N_x species), in which the high S_{BET} together with high mesoporosity could lead not only to efficient mass transport of reactants and/or products, but also to high exposure of catalytic sites [46,47]. Meanwhile, the highly dispersed active sites that are easily accessible to reactants are also a reason for the improved activity. Apart from 2-methylimidazole that involved in ZIF-67, also other ligands, such as α -diimine [30], benzimidazole [47], phthalocyanine [48], and histidine [49], were used to synthesize such Co-N/C catalysts.

Although considerable progress has been achieved in the preparation and application of Co-N/C catalysts, the catalytic performance and the precursor utilization efficiency are still needed to improve. Herein, we present a poly(Schiff base) precursor for the scalable synthesis of ultrahighly efficient Co-N/C catalyst with high mesoporosity for the selective CTH of nitroarenes using NaBH₄ as the hydrogen donor. The poly(Schiff base) precursor, namely POP-gm, was firstly synthesized by a facile, one-pot, Schiff base polycondensation of glyoxal and melamine in DMF in the presence of formic acid catalyst. After coordination to Co(II) ion, the obtained POP-gm/Co(II) complex was directly pyrolyzed at 950 °C, yielding Co-N/C-950 catalyst with a Co loading of 7.04 wt%. Benefiting from the porous structure and the strong Co(II)-binding affinity of POP-gm precursor, the as-fabricated Co-N/C-950 catalyst has a high S_{BET} value (865 m² g⁻¹) with external-porosity up to 98.8 %, a high N content with high proportions of pyrrolic-N, pyridinic-N and Co-N_x, together with highly dispersed Co(0) nanoparticles with average size below 20 nm. Considering the strong coordination interaction between Co atoms and pyridinic-N/pyrrolic-N, the high percentage of such N-configurations is helpful to stabilize Co species. In addition, the high external-porosity of Co-N/C-950 catalyst is also important to enhance its activity and stability, since smaller mesoporosity is crucial for the full exposure of active sites along with effective mass transfer, while bigger mesoporosity and macroporosity can act as the reservoirs for reactants, therefore favoring the CTH reaction. As a result, the Co-N/C-950 catalyst showed ultrahigh activity, selectivity, and stability for the CTH of nitroarenes with NaBH₄ as the hydrogen donor. More importantly, the Co(0) particles embedded in the Co-N/C-950 catalyst can be further transformed to Co₄N phase by a facile nitridation reaction. By comparison, the as-nitridated Co-N/C-950 catalyst (namely Co₄N-N/C-950) has an even higher activity for the CTH of 4-nitrophenol (4-NP), with an

ultrahigh turnover frequency (TOF) up to 310 mol_{4-NP} mol_{Co}⁻¹ min⁻¹.

2. Experiment section

2.1. Synthesis of POP-gm and POP-gm/Co(II) complex

In a typical synthesis (Scheme 1), melamine (19.1 g, 151 mmol), formic acid (10 mL), and DMF (700 mL) were added to a flask and stirred at 80 °C under a N₂ atmosphere. Then glyoxal (40 wt% aqueous solution, 26.0 mL, 229 mmol) was injected via a syringe. The reaction mixture was heated to reflux for 96 h, after cooling to room temperature, the resultant POP-gm was filtered, washed thoroughly with DMF and ethanol, and then dried in vacuum at 60 °C for 12 h (yield, 85 %). Subsequently, the as-synthesized POP-gm (10.0 g) was dispersed in 300 mL of dry DMF under a N₂ atmosphere, and then Co(NO₃)₂·6H₂O (10.0 g, 34.0 mmol) was added. The mixture was stirred at 80 °C for 4 h. After cooling to room temperature, the resulting POP-gm/Co(II) complex was filtered, washed with ethanol, and dried in vacuum.

2.2. Synthesis of Co-N/C-x catalysts

The as-synthesized POP-gm/Co(II) complex was separately pyrolyzed in a tube furnace at 850 °C, 950 °C, and 1050 °C for 2 h in a N₂ atmosphere at a heating rate of 4 °C min⁻¹. The resultant carbon products were washed with 1.0 M HCl aqueous solution at 60 °C for 2 h to remove CoO_x nanoparticles. After vacuum drying, the obtained Co/N-codoped porous carbons were named as Co-N/C-x (x = 850, 950, and 1050, denoting the pyrolysis temperatures). For comparison, Co/N-codoped carbon without washing with 1.0 M HCl was also prepared at 950 °C and was named as Co-CoO_x-N/C-950. In addition, N-doped carbon (namely N/C-950) was prepared by directly pyrolyzing POP-gm at 950 °C for 2 h in a N₂ atmosphere.

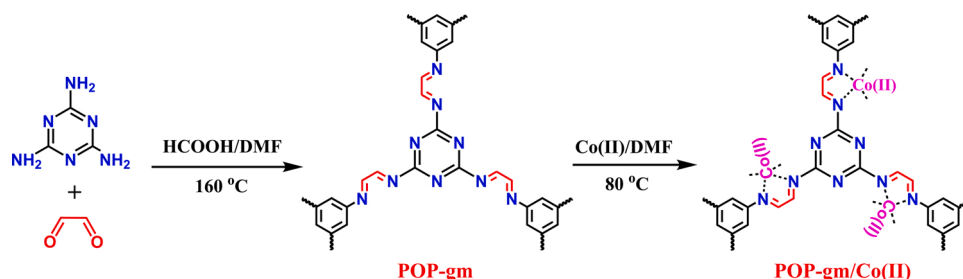
2.3. CTH of 4-nitrophenol (4-NP) to 4-aminophenol (4-AP)

In a typical experiment, the Co-N/C-950 catalyst (2.0 mg) was dispersed in 30 mL of 4-NP aqueous solution (18 mM, 0.54 mmol) by sonicating for 20 s followed by stirring at 25 °C. And then NaBH₄ (0.30 g, 8.0 mmol) was added into the mixture under vigorous stirring, the reaction progress was monitored by UV-vis spectroscopy.

3. Results and discussion

3.1. Synthesis and characterization of Co-N/C-x catalysts

In this study, the POP-gm precursor was synthesized by formic acid-catalyzed Schiff base condensation of glyoxal and melamine in DMF (Scheme 1). The formation of imine-linked, porous polymeric network was verified by FT-IR spectroscopy and porosity analysis. As illustrated in Fig. S1, a strong imine (C=N) stretch at 1628 cm⁻¹ was observed for POP-gm [50], clearly confirming the generation of C=N bonds in the polymeric network. The N₂ adsorption/desorption analysis indicated that the S_{BET} and total pore volume (V_t) values were around 281 m² g⁻¹ and 0.612 cm³ g⁻¹, respectively, for the POP-gm (Fig. S2). Given the strong coordination ability of Schiff base toward transition metal ions, the coordination of POP-gm to Co(NO₃)₂ was performed at 80 °C in dry DMF, yielding POP-gm/Co(II) complex (Scheme 1). The formation of POP-gm/Co(II) complex was also characterized by FT-IR spectroscopy and porosity analysis. As expected, the imine (C=N) stretch at 1628 cm⁻¹ for free POP-gm was shifted to 1596 cm⁻¹ after the coordination to Co(II) ion [50] (Fig. S1), whereas the S_{BET} and V_t values were reduced to 91 m² g⁻¹ and 0.286 cm³ g⁻¹, respectively, for the POP-gm/Co(II) complex (Fig. S2). And meanwhile, the mesopore-size of the complex became smaller by comparison with the free POP-gm, confirming the pore-filling of Co(II) in POP-gm network. The Co loading in the POP-gm/Co(II) complex was determined by TGA analysis. Compared



Scheme 1. Schematic illustration of the synthesis of POP-gm and POP-gm/Co(II) complex.

with free POP-gm, the coordinated POP-gm network showed a mass retention of 19.1 % under an air atmosphere (Fig. S3), which corresponded to Co_3O_4 owing to air oxidation at elevated temperature. Accordingly, the Co loading in POP-gm/Co(II) complex was estimated to be 14.0 wt%.

The POP-gm/Co(II) complex was then pyrolyzed at 850–1050 °C followed by dilute acid leaching to give Co-N/C-*x* catalysts, where *x* denotes the pyrolysis temperature. During the pyrolysis of POP-gm/Co(II) complex, POP-gm network was converted to N-doped carbon, while Co(II) salt was transformed into Co-N_{*x*} species, and Co(0)/CoO_{*x*} nanoparticles. And simultaneously, the in-situ formed Co(0) nanoparticles catalyzed the generation of N-doped graphitic carbon. After washing with 1.0 M HCl aqueous solution, the redundant CoO_{*x*} nanoparticles were removed, yielding the final Co-N/C-*x* catalysts (Fig. S4). Owing to that the synthesis conditions can exert a great impact on the catalytic performance of Co-N/C-*x* catalysts, the Co(II) loading and

pyrolysis temperature were optimized and verified to be 14.0 wt% and 950 °C, respectively, by which the catalytic activity in CTH of 4-NP with NaBH₄ donor was used as the criterion (Fig. S5). Comparatively, pyrolysis temperature has a greater impact on the catalytic activity; therefore, the structure and catalytic properties of the Co-N/C-*x* catalysts will be investigated in detail.

The powder X-ray diffraction (PXRD) analysis was firstly utilized to characterize the Co-N/C-*x* catalysts. As shown in Fig. 1a, all Co-N/C-*x* catalysts show diffraction peaks at $2\theta = 22^\circ$, 44.2° , 51.4° , and 75.7° , in which the broad peak at $2\theta = 22^\circ$ can be assigned to the turbostratic carbon caused by N-doping [51,52], while the weak but sharp peaks at $2\theta = 44.2^\circ$, 51.4° , and 75.7° can be ascribed to (111), (200), and (220) crystal planes of Co(0) particles (JCPDS no. 15-0806) [53,54]. On the other hand, the diffraction peaks arising from CoO_{*x*} species cannot be detected, suggesting the complete removal of CoO_{*x*} nanoparticles during the acid leaching. In contrast, the unleached catalysts (namely

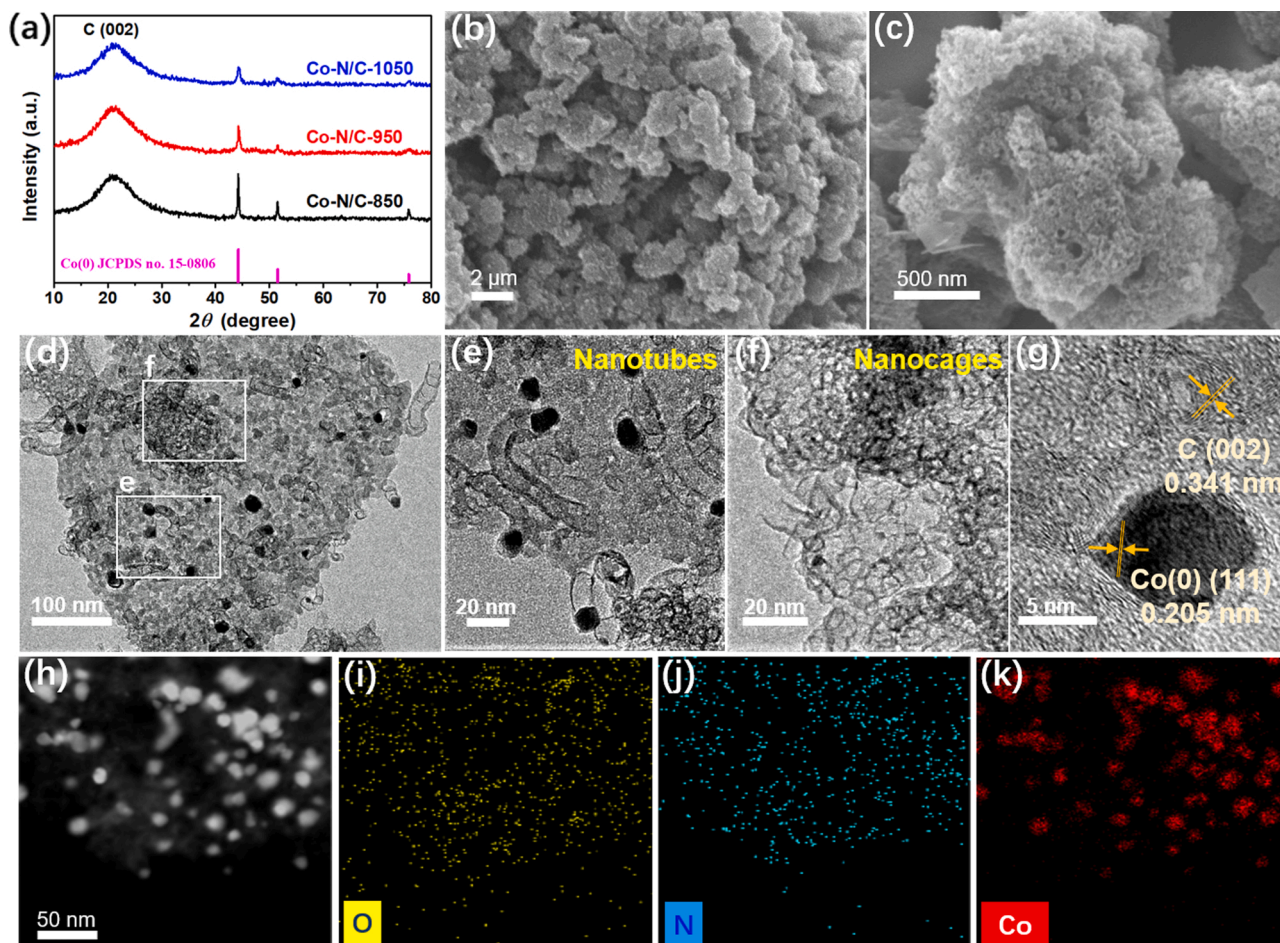


Fig. 1. PXRD patterns of Co-N/C-*x* catalysts (a). SEM (b, c), TEM (d-f), HRTEM (g), and EDX elemental mapping images (h-k) of Co-N/C-950 catalyst.

Co-CoO_x-N/C-x) clearly indicated the presence of CoO_x species (Fig. S4). The scanning electron microscopy (SEM) images of Co-N/C-x catalysts are shown in Fig. 1b, c and Fig. S6. As seen, the carbon matrices are the aggregation of irregular particles that range from 500 nm to 2 μm, almost independent of the pyrolysis temperature. At high magnification, short nanotubes are also seen on the surface of the aggregates (Fig. 1c and Fig. S6). The transmission electron microscopy (TEM) image of Co-N/C-950 catalyst confirms that the carbon matrix is actually composed of short carbon nanotubes and carbon nanocages (Fig. 1d), within which Co(0) nanoparticles with particle size of 5–20 nm are homogeneously embedded. At high magnification, carbon nanotubes with an average diameter of ~15 nm are clearly visible, in which Co(0) nanoparticles are encapsulated in the nanotube tips (Fig. 1e). In addition, carbon nanocages are also visible at high magnification (Fig. 1f). These results indicate that Co-N/C-950 catalyst is an aggregation of all kinds of short carbon nanotubes and carbon nanocages. High-resolution TEM (HRTEM) of Co-N/C-950 catalyst in Fig. 1g shows both lattice fringes for the (111) facet of Co(0) nanoparticles (0.205 nm) and for the (002) lattice plane of graphitic carbon (0.341 nm), in good agreement with PXPD analysis. In addition, energy-dispersive X-ray (EDX) elemental mapping images of the Co-N/C-950 catalyst indicate that the O, N, and Co elements are uniformly distributed in this catalyst (Fig. 1i-k).

The X-ray photoelectron spectroscopy (XPS) was then conducted to analyze the Co- and N-doping configurations of the Co-N/C-x catalysts. As shown in Fig. 2a, the full-scan XPS spectra confirmed again the presence of C, N, O, and Co elements in all Co-N/C-x catalysts, whose contents are dependent on the pyrolysis temperature and higher pyrolysis temperature leads to a decrease in both superficial Co and N

contents, i.e., the superficial Co/N contents are around 3.65/7.24 at%, 1.68/4.80 at%, and 1.35/4.38 at%, respectively, for Co-N/C-850, Co-N/C-950, and Co-N/C-1050 catalysts (Table S1). This is due to the fact that higher pyrolysis temperature can not only accelerate the cleavage of C–N bonds, also can promote the formation of aggregated Co(0) and CoO_x nanoparticles, of which the CoO_x nanoparticles were removed by acid leaching [55,56]. Worth noting is that the Co loading determined by XPS analysis is slightly lower than that detected by inductively coupled plasma optical emission spectrometry (ICP-OES), i.e., 15.08 wt%, 7.04 wt%, and 5.05 wt%, respectively, for the Co-N/C-850, Co-N/C-950, and Co-N/C-1050 catalysts (Table S1). The bonding configurations of N- and Co-doping in these catalysts were investigated by deconvoluting N 1s and Co 2p XPS spectra. The deconvoluted N 1s spectra suggest the presence of pyridinic-N (398.1 eV), Co-N_x (398.9 eV), pyrrolic-N (400.5 eV), and graphitic-N (401.2 eV) in all the Co-N/C-x catalysts [53] (Fig. 2b), whose contents are also related to the pyrolysis temperature. With the increase of pyrolysis temperature, the graphitic-N content rose significantly, whereas the pyridinic-N and pyrrolic-N contents exhibited an opposite trend. As a consequence, the content of Co-N_x configuration reached the maximum at 950 °C (Fig. 2d), which is in agreement with previous studies [54,57,58]. In addition, the deconvoluted Co 2p_{3/2} spectra indicate the existence of Co 2p_{3/2} (778.0 eV), Co^{x+} 2p_{3/2} (780.0 eV) [53,54] (Fig. 2c), which are also temperature-dependent (Table S2). Although the peak for Co-N_x configuration cannot be unequivocally deconvoluted, it is quite clear that Co-doping in the Co-N/C-x catalysts mainly exists in the form of Co(0) nanoparticles and Co-N_x species, which can be further verified by the deconvoluted O 1s XPS spectra (Fig. S7).

The porosities of the Co-N/C-x catalysts were finally evaluated by N₂

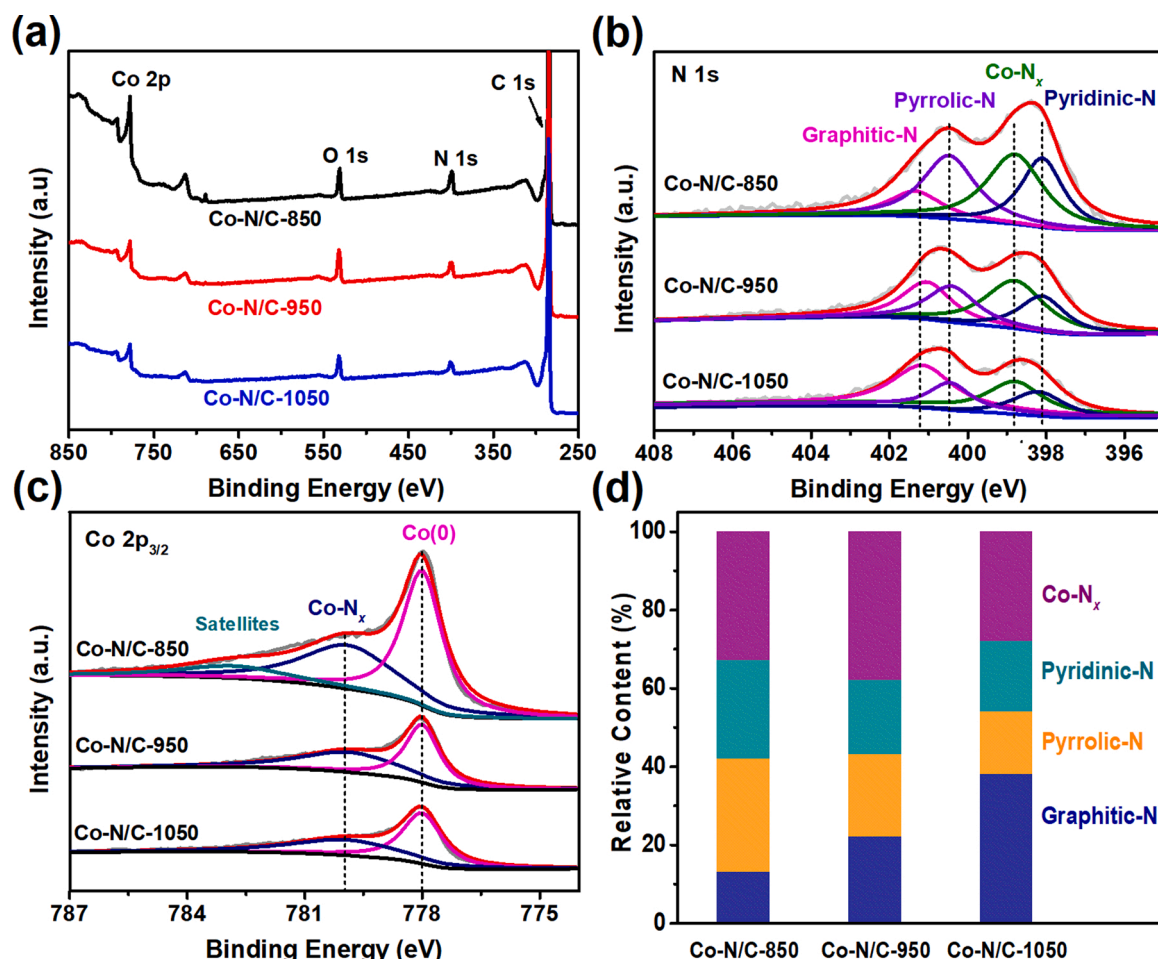


Fig. 2. XPS survey (a) and high-resolution N 1s (b), Co 2p_{3/2} (c) XPS spectra and the relative contents of N-bonding configurations (d) of Co-N/C-x catalysts.

adsorption/desorption analysis. As depicted in Fig. 3a, all Co-N/C-*x* catalysts exhibited type IV isotherms, accompanying with H3 hysteresis loops and rapid N₂ uptakes at p/p_0 near to 1.0, indicating the copresence of meso- and macroporosity [59]. The pore-size distributions of the Co-N/C-*x* catalysts shown in Fig. 3b provided further evidence, in which broad pore-size distributions that range from 2.0 nm to 200 nm can be observed. The S_{BET} and V_t values are determined to be 488.0 m² g⁻¹/0.784 cm³ g⁻¹, 865.0 m² g⁻¹/1.614 cm³ g⁻¹, and 516.0 m² g⁻¹/0.922 cm³ g⁻¹, respectively, for the Co-N/C-850, Co-N/C-950, and Co-N/C-1050 catalysts (Table S3). Obviously, both S_{BET} and V_t values are directly related to the pyrolysis temperature, in which the optimum pyrolysis temperature was 950 °C that yielded the largest S_{BET} and V_t values. At lower or higher pyrolysis temperatures, however, both S_{BET} and V_t values decreased owing to that the lower pyrolysis temperature would result in incomplete pyrolysis, whereas the higher pyrolysis temperature would lead to the collapse of carbon skeletons, and in both cases, S_{BET} and V_t values tended to decline. Notably, the as-synthesized Co-N/C-*x* catalysts were actually meso-/macro-porous materials as evidenced by the extremely high external-porosity (defined as V_e/V_t , V_e is the external pore volume), i.e., 97.7 %, 98.8 % and 99.6 %, respectively, for the Co-N/C-850, Co-N/C-950, and Co-N/C-1050 catalysts (Table S3). Especially, the high S_{BET} and V_t values along with the extremely high external-porosity of Co-N/C-950 catalyst can ensure the high activity and high stability, because mesoporosity in the range of 2–5 nm is beneficial for both active-site exposure and mass transport, while pores above 5 nm can not only facilitate the mass transfer, but also act as the reservoirs for both reactants and products, thus leading to a better catalytic performance [34,60].

3.2. Catalytic performance of Co-N/C-*x* catalysts

The catalytic performance of the Co-N/C-*x* catalysts for the CTH of nitroarenes was first estimated by using a 4-NP/NaBH₄ aqueous system in an air atmosphere, which has been regarded as the benchmark for assessing the catalytic activities of heterogeneous catalysts [61]. Due to the extremely high catalytic activity of our Co-N/C-*x* catalysts, the amounts of added catalyst and NaBH₄ in our case were greatly reduced in comparison with those reported in the literature (Table S5). The CTH of 4-NP was thus performed by adding 2.0 mg of Co-N/C-*x* catalysts to a solution (30 mL) containing 4-NP (18 mM, 0.54 mmol) and NaBH₄ (0.30 g, 8.0 mmol). Notably, the limited use of NaBH₄ is also beneficial for environmental protection by decreasing NaBO₂ release. In such a case, UV-vis spectroscopy was used to quantitatively monitor the CTH of 4-NP to 4-aminophenol (4-AP) with NaBH₄. With the assistance of Co-N/C-*x* catalysts, the 4-NP could be very quickly and quantitatively converted to 4-AP as evidenced by a rapid decrease in 4-NP ion peak at 400 nm and a rapid increase in 4-AP peak at 300 nm (Fig. 4a and Fig. S8a, S9a). In addition, full chemoselectivity was also confirmed by the four isobestic points at 224, 244, 281, and 313 nm [62]. The

turnover frequency (TOF) values are determined to be 46, 226, and 105 mol_{4-NP} mol_{Co}⁻¹ min⁻¹, respectively, for the Co-N/C-850, Co-N/C-950, and Co-N/C-1050 catalysts at 25 °C based on the Co contents detected by the ICP-OES analysis (Fig. 4b and Fig. S8b, S9b).

The kinetics and apparent activation energy (E_a) for the CTH of 4-NP by using the Co-N/C-*x* catalysts were then investigated. In the current case, the amounts of added catalysts have halved for the purpose of evaluating the conversion more precisely. The rate constants (k) can be calculated from the plots of $\ln(C_t/C_0)$ versus reaction time t , where C_0 and C_t are the 4-NP concentrations at reaction time $t = 0$ and $t = t$, respectively. In agreement with previous studies [63,64], the pseudo-first-order kinetics was observed for the CTH of 4-NP under the catalysis of Co-N/C-*x* catalysts as confirmed by the linear plots of $\ln(C_t/C_0)$ versus t , in which the induction period was not observed in all the CTH reactions (Fig. S10-S13). Owing to the fact that the k value relies strongly on the amount of the used catalysts, herein activity parameter, k_c , is used instead of the k by taking into account the concentration of catalyst (C_c) in L g⁻¹, i.e., $k_c = k/C_c$ in L g⁻¹ s⁻¹, as suggested by Thünnemann and Kästner [65]. The k_c values were thus calculated to be 0.324 L g⁻¹ s⁻¹, 0.727 L g⁻¹ s⁻¹, and 0.250 L g⁻¹ s⁻¹, respectively, for the Co-N/C-850, Co-N/C-950, and Co-N/C-1050 catalysts (Table S4). In addition, the E_a values can also be determined from the plots of $\ln(k_c)$ versus $10^3/T$ (T is Kelvin temperature), and are estimated to be 26.10 kJ mol⁻¹, 24.94 kJ mol⁻¹, and 28.60 kJ mol⁻¹, respectively, for the CTH of 4-NP over the Co-N/C-850, Co-N/C-950, and Co-N/C-1050 catalysts (Fig. S13 and Table S4).

Besides the catalytic activity, the reusability of a heterogeneous catalyst is another important factor for practical application. The recyclability of the Co-N/C-950 catalyst was then tested under optimized conditions. Generally, an aqueous solution (30 mL) of 4-NP (18 mM, 0.54 mmol) and Co-N/C-950 catalyst (2.0 mg) was sonicated for 20 s followed by stirring at 25 °C. Then, NaBH₄ (0.30 g, 8.0 mmol) was added and stirred for another 2 min. After that, the Co-N/C-950 catalyst was recovered by centrifugation followed by washing with water and methanol. The solid catalyst was allowed to be placed in the flask for the next cycle after being dried under high vacuum. As shown in Fig. 4c, the activity and selectivity remained almost unchanged after 20 cycles, suggesting the excellent reusability. In order to further demonstrate the stability, the recovered Co-N/C-950 catalyst was characterized by PXRD and ICP-OES analyses. As depicted in Fig. S14, the XRD pattern of recovered catalyst was almost identical to that of fresh Co-N/C-950 catalyst. Moreover, ICP-OES analysis of the recovered catalyst after 20th cycle indicated that Co leaching was only around 500 ppm, confirming the extremely high stability of the Co-N/C-950 catalyst.

The selectivity of the Co-N/C-950 catalyst was also investigated by the CTH of a variety of functionalized nitroarenes under the optimized reaction conditions. As depicted in Table 1, a variety of functionalized nitroarenes were selectively hydrogenated to the corresponding aminoarenes in good yields over the Co-N/C-950 catalyst (Fig. S15-S16). For

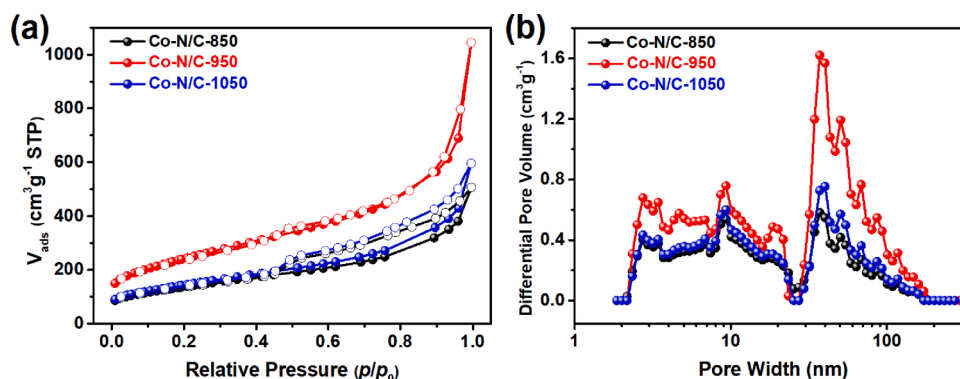


Fig. 3. (a) N₂ adsorption/desorption isotherms and (b) pore-size distribution curves of Co-N/C-*x* catalysts.

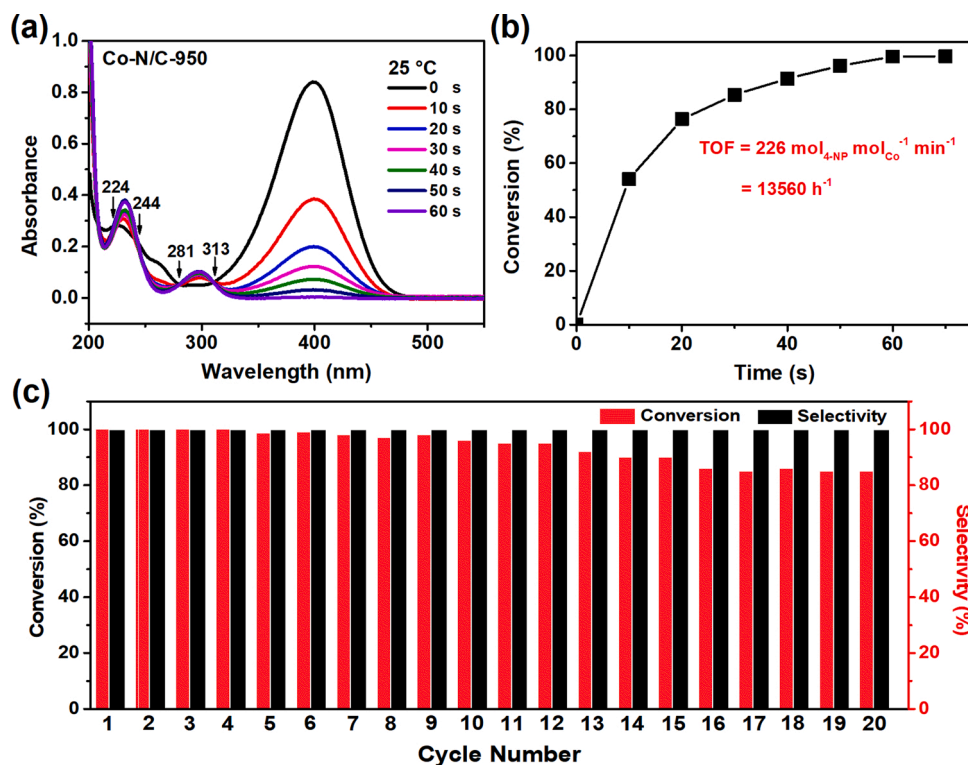


Fig. 4. (a) UV-vis absorption spectra for the CTH of 4-NP in the presence of Co-N/C-950 catalyst and (b) plot of conversion versus reaction time. Reaction conditions: catalyst (2.0 mg), 4-NP (30 mL, 18 mM), NaBH₄ (0.30 g, 8.0 mmol), 25 °C, reaction time $t = 60$ s. (c) Recyclability of Co-N/C-950 catalyst for the CTH of 4-NP.

example, halonitroarenes could be hydrogenated to the corresponding haloaminoarenes in high yields and high selectivities, in which the dehalogenation reactions were not observed. In addition, nitroarenes bearing reducible functionalities, such as olefin, nitrile, aldehyde, keto, ester, amino, and carboxyl, were also converted smoothly to aminoarenes in high yields and high chemoselectivities.

To better understand the synergistic effect of Co/N-codoping and the possibly active sites in Co-N/C-950 catalyst, a series of control experiments were conducted. But before that, it is reasonable to assume that the possibly active sites in Co-N/C-950 catalyst are Co-N_x species, Co(0) nanoparticles, and N-C configurations based on previous studies [5,22,24,66,67], even though their contributions cannot be precisely assessed. In order to demonstrate the role of Co-doping in the Co-N/C-950 catalyst, the catalytic performance of the N/C-950 catalyst (prepared by directly pyrolyzing POP-gm at 950 °C) was examined in aqueous 4-NP/NaBH₄ system, in which the time needed to complete the conversion of 4-NP could be up to 36 min (Fig. S17). This result suggests that the catalytic contribution of N-C configurations is less or negligible by comparison with Co-doping in the Co-N/C-950 catalyst, which in turn proves that Co-N_x species and Co(0) nanoparticles should be primarily responsible for the high activity. In our case, the contribution of CoO_x nanoparticles can be excluded because the Co-N/C-950 catalyst was preleached in diluted HCl aqueous solution and CoO_x species were completely removed as evidenced by PXRD analysis (see Fig. 1a). In addition, both Co-CoO_x-N/C-950 (unleached) and Co-N/C-950 (leached) catalysts showed almost identical activity in NaBH₄-participated CTH of 4-NP (Fig. S18), further confirming that the CoO_x nanoparticles have negligible contribution to this CTH reaction. In this context, it is evident that the mainly active sites are Co-N_x species and Co(0) nanoparticles. Their catalytic contributions were thus roughly assessed by a second acid-washing experiment. In the second washing step, the Co-N/C-950 catalyst was re-washed with 2.0 M H₂SO₄ solution at 80 °C for 72 h (namely Co-N/C-950H₁), during which the Co(0) nanoparticles were completely removed but the Co-N_x sites were retained as confirmed by PXRD and XPS analyses (Fig. 5a, b). Owing to

the removal of Co(0) nanoparticles, the Co-N/C-950H₁ catalyzed CTH reaction showed a lower 4-NP conversion (81 %) within the same period of reaction time (Fig. 5c, d), revealing a declined activity. In other words, a long period of time was required to complete such a CTH reaction. According to the 4-NP conversions that obtained under the catalysis of Co-N/C-950 and Co-N/C-950H₁ catalysts, a difference of 19 % was observed, which indicates that the catalytic contribution of Co(0) nanoparticles is around 19 % (Fig. 5d). Similarly, the N/C-950 catalyzed CTH reaction yielded a 4-NP conversion of 18 % within the same period of reaction time, revealing the catalytic contribution of N-C configurations is about 18 % (Fig. 5d). By comparison of the 4-NP conversions obtained with the Co-N/C-950H₁ and with the N/C-950 catalysts, the contribution of Co-N_x species is estimated to be 63 % (Fig. 5d). Notably, such rough estimations did not take into account the differences between porosities (i.e., S_{BET} and V_p) and/or N-doping (i.e., N-C configurations and their relative contents) in the Co-N/C-950, Co-N/C-950H₁, and N/C-950 catalysts. Nevertheless, these results confirm that the Co-N_x species plays a pivotal role in the Co-N/C-950 catalyst and is mainly responsible for the ultrahigh activity. Such a conclusion was also supported by previous experimental and theoretical studies [24,68–72], in which the high activity of Co-N_x sites in the CTH of 4-NP have been well demonstrated. In our case, although N-C configurations in the Co-N/C-950 catalyst contribute less to the catalytic activity, the N-doping (both content and configuration) still plays an important role since such a high activity of this catalyst can not be achieved with such a low Co loading (7.04 wt%, obtained by ICP-OES analysis). Besides, the contribution of high S_{BET} and high porosity in the Co-N/C-950 catalyst also cannot be ignored.

To further demonstrate the catalytic contribution of Co-N_x species, SCN⁻(L₁)-poisoning experiment was firstly conducted on both Co-N/C-950 and Co-N/C-950H₁ catalysts (namely Co-N/C-950L₁ and Co-N/C-950H₁L₁) since the SCN⁻ can block Co-N_x sites through coordination interaction [73], while Co(0) nanoparticles can remain intact. Therefore, it seems logical to conclude that the differences of 4-NP conversion between the Co-N/C-950- and Co-N/C-950L₁-catalyzed CTH reactions

Table 1
CTH of various nitroarenes catalyzed by the Co-N/C-950 catalyst.

Entry	Substrate	Product	Reaction time	Conv. (%) ^a	Sel. (%) ^a
1			2 min	> 99 (99)	> 99 (99)
2			2 min	> 99 (99)	> 99 (99)
3			2 min	> 99 (99)	> 99 (99)
4			4 min	> 99 (99)	> 90 (84)
5			4 min	> 99 (99)	> 99 (99)
6			4 min	> 99 (99)	> 99 (99)
7			2 min	> 99 (99)	> 99 (99)
8			4 min	> 99 (99)	> 99 (99)
9			4 min	> 99 (99)	> 99 (99)
10			5 min	> 99 (80)	> 90 (90)

Reaction conditions: Co-N/C-950 (2.0 mg), nitroarenes (30 mL, 3.0 mM), NaBH₄ (0.10 g, 2.6 mmol), ethanol/H₂O (9/1, v/v), 25 °C.

^a Conversion and selectivity were determined by UV-vis (outside the parentheses) and HPLC (inside the parentheses) analyses.

should equal approximately to that of the Co-N/C-950H₁- and Co-N/C-950H₁L₁-catalyzed CTH reactions, and that Co-N/C-950H₁L₁ catalyst should show an activity comparable to the N/C-950 catalyst due to that the Co-containing active sites were either being removed or being deactivated. However, the conversion of 4-NP over the Co-N/C-950H₁L₁ catalyst is significantly higher than that over the N/C-950 catalyst, i.e., 66 % versus 18 %, within the same period of reaction time, although the difference of 4-NP conversion between Co-N/C-950- and Co-N/C-950L₁-catalyzed CTH reactions equals approximately to that of Co-N/C-950H₁- and Co-N/C-950H₁L₁-catalyzed CTH reactions (Fig. S19), indicating that the L₁-poisoning cannot completely block the Co-N_x sites. In this case, disodium ethylenediamine tetraacetate (EDTA-2Na, L₂) that can form more stable complex with Co-N_x sites was used to poison such catalysts. The stability constants (lgβ₁) of Co(II)/L₁ and Co(II)/L₂ complexes are around -0.04 and 16.31 [74], respectively. The L₂-poisoned Co-N/C-950 and Co-N/C-950H₁ catalysts are named as Co-N/C-950L₂ and Co-N/C-950H₁L₂, respectively. Although L₂ can block more Co-N_x sites by comparison with L₁, the Co-N_x sites still cannot be completely blocked due to that the selected L₂ is not strong enough to complex all the Co-N_x sites on the one hand, on the other hand, the coordinative saturation of Co-N_x sites would no longer interact with the L₂ (Fig. S20). In such a case, a third acid washing of Co-N/C-950H₁ catalyst was performed under harsh conditions, i.e., 9 M HNO₃ aqueous solution at 90 °C for 48 h (namely Co-N/C-950H₂), all the

Co-N_x sites could be removed [75], and left behind the catalytic activity that was similar to the N/C-950 catalyst (Fig. S21). Also, if the harsh HNO₃-washing was conducted directly on the Co-N/C-950 catalyst (namely Co-N/C-950Hh), all the Co(0) nanoparticles and Co-N_x sites can also be removed, yielding the Co-N/C-950Hh catalyst with a activity similar to both N/C-950 and Co-N/C-950H₂ catalysts (Fig. S21). These results confirm again that the catalytic contribution of Co-N_x sites is around 63 % in the Co-N/C-950 catalyst.

In order to further boost the catalytic activity of the Co-N/C-950 catalyst, this catalyst was nitridated at 600 °C for 4 h under dry NH₃ flow. As such, NH₃ was expected to react with Co(0) nanoparticles to generate Co nitride (Co₄N), yielding a nitridated catalyst that was named as Co₄N-N/C-950. The PXRD pattern of Co₄N-N/C-950 shows characteristic peaks at 2θ = 43.7°, 50.8°, and 74.9° (Fig. 6a), which can be assigned to (111), (200), and (220) crystal planes of Co₄N phase (JCPDS no. 41-0943) [76], indicating that the Co(0) nanoparticles in the Co-N/C-950 catalyst can be completely transformed into Co₄N phase. HRTEM images of the Co₄N-N/C-950 catalyst also shows lattice fringe for the (111) facet of Co₄N phase (0.207 nm) [77] (Fig. 6b), in good agreement with PXP analysis and proving further evidence for the Co₄N structure. XPS analysis of Co₄N-N/C-950 catalyst demonstrates that the superficial N content increases from 4.80 at% for the Co-N/C-950 catalyst to 6.19 at% for the nitridated catalyst (Table S1), in which the relative content of Co-N_x (398.9 eV) species increases but the relative contents of pyridinic-N (398.1 eV), pyrrolic-N (400.5 eV), and graphitic-N (401.2 eV) remain almost unchanged as confirmed by the deconvoluted N 1s peak (Fig. 6c). In addition, the peak located at 778.0 eV (Co(0)) for Co-N/C-950 catalyst was shifted to 778.2 eV after nitridation, accompanying with the decrease in intensity (Fig. 6d). On the contrary, the peak intensity at 780.0 eV, corresponding to Co-N_x species [78], increased obviously after nitridation (Fig. 6d). These results suggest that nitridation reaction of Co-N/C-950 can not only create the Co₄N structure, but also generate additional N-bonding configurations.

The catalytic activity of the Co₄N-N/C-950 catalyst for the CTH of nitroarenes was finally evaluated by using the 4-NP/NaBH₄ aqueous system. As shown in Fig. 7a, b and Video S1, the 4-NP can be quantitatively and selectively hydrogenated to 4-AP under the catalysis of Co₄N-N/C-950 catalyst with a TOF value as high as 310 mol_{4-NP} mol_{Co}⁻¹ min⁻¹ at 25 °C. Notably, such a TOF value is the highest reported to date for the transition metal-based heterogeneous catalysts participated 4-NP/NaBH₄ CTH system (Table S5). In addition, the *k_c* and *E_a* values were determined to be 1.238 L g⁻¹ s⁻¹ and 15.08 kJ mol⁻¹, respectively, for the Co₄N-N/C-950 catalyst in comparison with 0.727 L g⁻¹ s⁻¹ and 24.94 kJ mol⁻¹ for the Co-N/C-950 catalyst (Fig. 7c, d, Fig. S23, and Table S4). The lower *E_a* value of the Co₄N-N/C-950 catalyst can be explained by the high conductivity of Co₄N structure [79,80] that facilitates the electron transfer from BH₄⁻ anion to 4-NP. Besides, the intrinsically high activity of the Co₄N structure has also been demonstrated by previous experimental and theoretical studies [81,82].

4. Conclusions

In summary, a series of Co/N-codoped porous carbon (Co/N-C) catalysts were synthesized by directly pyrolyzing poly(Schiff base)/Co (II) complex at elevated temperatures. The strong Co(II)-binding affinity of poly(Schiff base) led to the formation of uniformly distributed Co- and N-doping configurations. The Co-N_x species has been demonstrated to be highly active in the CTH of nitroarenes and the catalytic contributions of Co-N_x species, Co(0) nanoparticles and N-C configurations were confirmed and roughly estimated by the acid-etching and the ligand-poisoning experiments. The as-synthesized Co-N/C-950 catalyst exhibited ultrahigh catalytic activity for the CTH of 4-nitrophenol (4-NP) with a turnover frequency up to 226 mol_{4-NP} mol_{Co}⁻¹ min⁻¹ together with an extremely high stability. In addition, the Co-N/C-950 catalyst also displayed high activity and high chemoselectivity for the CTH of nitroarenes bearing reducible functionalities. Moreover, the Co(0)

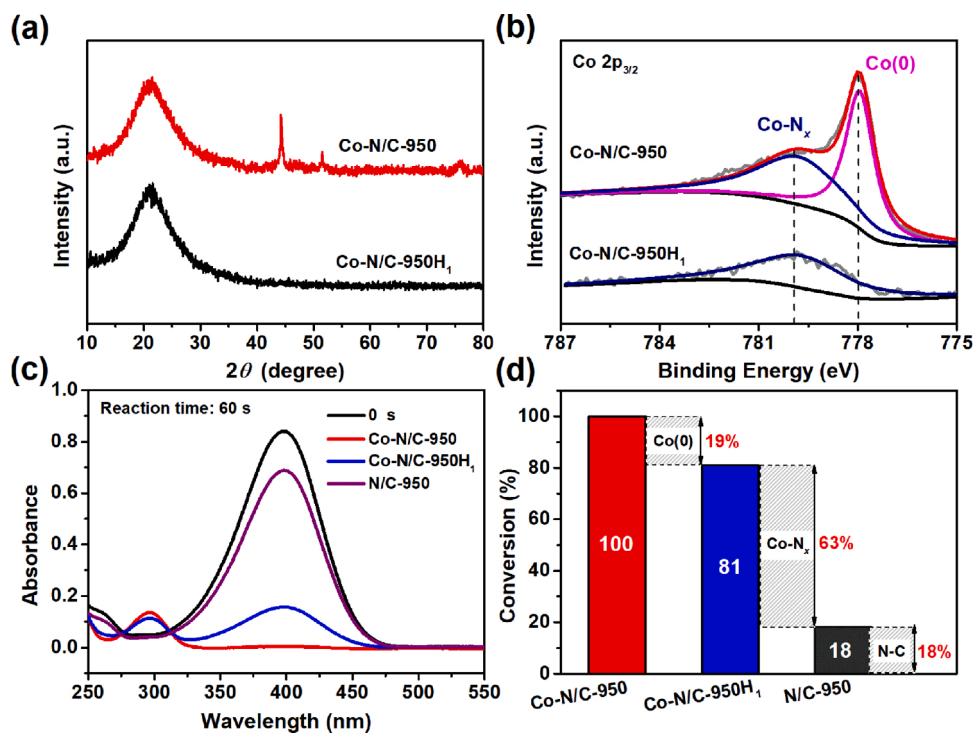


Fig. 5. PXRD patterns (a) and high-resolution Co 2p_{3/2} XPS spectra (b) of Co-N/C-950 and Co-N/C-950H₁ catalysts. UV-vis absorption spectra (c) and the 4-NP conversions (d) for the CTH of 4-NP in the presence of Co-N/C-950, Co-N/C-950H₁, and N/C-950 catalysts. Reaction conditions: Co-N/C-950 (2.0 mg), 4-NP (30 mL, 18 mM), NaBH₄ (0.30 g, 8.0 mmol), reaction time $t = 60$ s, 25 °C. The amounts of other catalysts were tuned by considering the acid-leached Co.

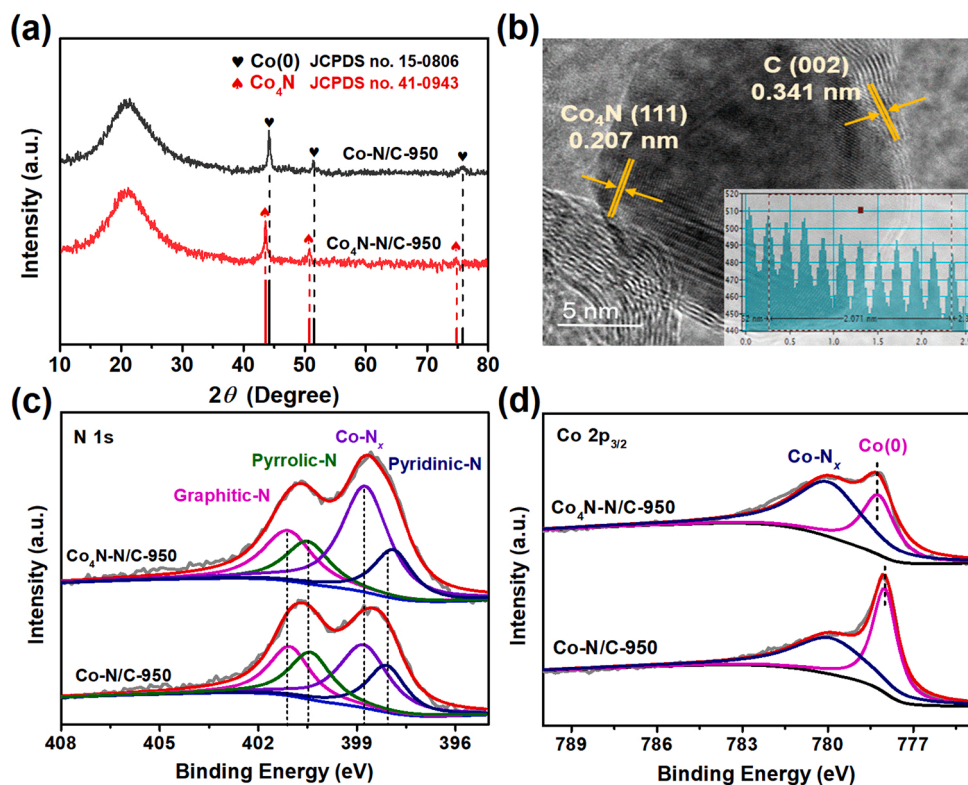


Fig. 6. PXRD patterns (a) and high-resolution N 1s (c) and Co 2p_{3/2} (d) XPS spectra of Co-N/C-950 and Co₄N-N/C-950 catalysts. (b) TEM image of Co₄N-N/C-950 catalyst, inset in (b) indicates the lattice parameter of Co₄N phase.

particles embedded in the Co-N/C-950 catalyst were successfully transformed to Co₄N phase by a facile nitridation reaction. The as-obtained Co₄N-N/C-950 catalyst had a much higher activity than that

of Co-N/C-950 catalyst, with a turnover frequency of 310 mol_{4-NP} mol_{Co}⁻¹ min⁻¹ for the CTH of 4-NP.

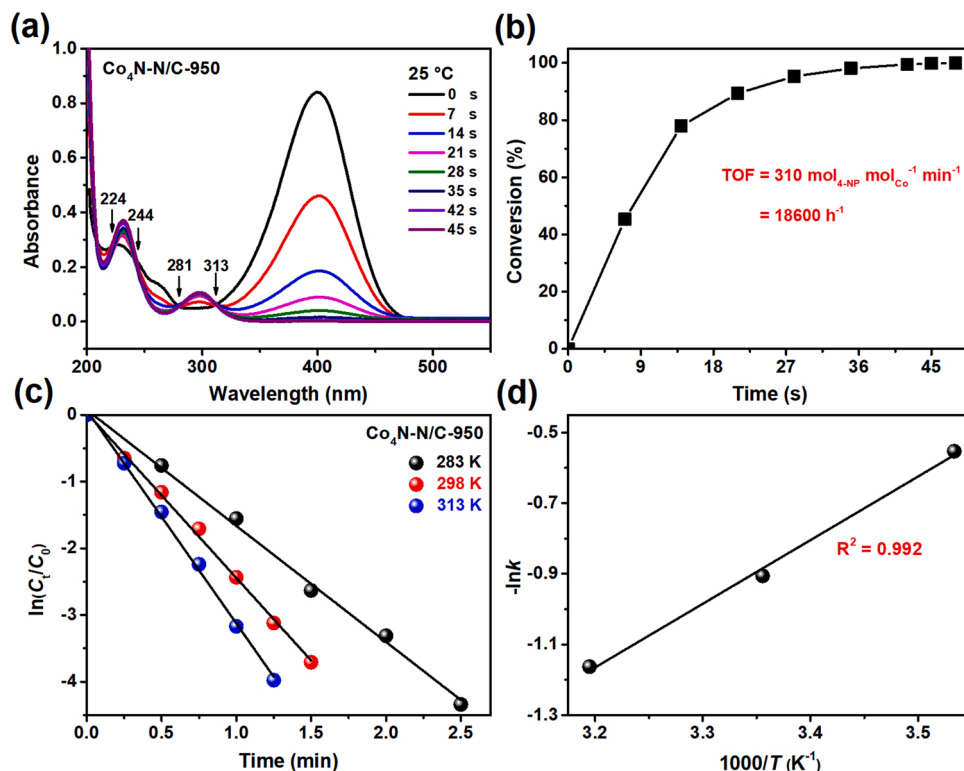


Fig. 7. (a) UV-vis absorption spectra for the CTH of 4-NP in the presence of $\text{Co}_4\text{N-N/C-950}$ catalyst and (b) plot of conversion versus reaction time. Reaction conditions: catalyst (2.0 mg), 4-NP (30 mL, 18 mM), NaBH_4 (0.30 g, 8.0 mmol), 25 °C. (c) Plots of $\ln(C_t/C_0)$ versus reaction time for the CTH of 4-NP with $\text{Co}_4\text{N-N/C-950}$ at different temperatures and (d) plot of $-\ln k$ against $10^3/T$. The reaction conditions are the same as above, except for the amount of catalyst (1.0 mg) that is used.

CRediT authorship contribution statement

Weichao Xie: Conceptualization, Data curation, Formal analysis, Investigation, Methodology, Writing-original draft. **Bei Liu:** Data curation. **Yijiang Liu:** Data curation. **Hongbiao Chen:** Formal analysis, Writing-review & editing. **Mei Yang:** Data curation. **Huaming Li:** Project administration, Designed the study, Writing-review & editing.

Declaration of Competing Interest

The authors report no declarations of interest.

Acknowledgments

Financial support from Program for NSFC (51674219), Hunan Provincial Innovation Foundation for Postgraduate (CX2018B367) and the Construct Program of the Key Discipline in Hunan Province is greatly acknowledged.

Appendix A. Supplementary data

Supplementary material related to this article can be found, in the online version, at doi:<https://doi.org/10.1016/j.apcata.2021.118249>.

References

- C. Van Nguyen, S. Lee, Y.G. Chung, W.H. Chiang, K.C.W. Wu, *Appl. Catal. B Environ.* 257 (2019), 117888, <https://doi.org/10.1016/j.apcatb.2019.117888>.
- L. Liu, Q. Zhao, R. Liu, L. Zhu, *Appl. Catal. B Environ.* 252 (2019) 198–204, <https://doi.org/10.1016/j.apcatb.2019.04.026>.
- Y. Ai, Z. Hu, L. Liu, J. Zhou, Y. Long, J. Li, M. Ding, H.B. Sun, Q. Liang, *Adv. Sci.* 6 (2019), 1802132, <https://doi.org/10.1002/advsc.201802132>.
- R.M. Penner, *Acc. Chem. Res.* 50 (2017) 1902–1910, <https://doi.org/10.1021/acs.accounts.7b00163>.
- F. Wang, S. Song, K. Li, J. Li, J. Pan, S. Yao, X. Ge, J. Feng, X. Wang, H. Zhang, *Adv. Mater.* 28 (2016) 10679–10683, <https://doi.org/10.1002/adma.201603608>.
- R. Yun, W. Ma, S. Wang, W. Jia, B. Zheng, *Inorg. Chem.* 58 (2019) 6137–6142, <https://doi.org/10.1021/acs.inorgchem.9b00385>.
- M. Yuan, Y. Long, J. Yang, X. Hu, D. Xu, Y. Zhu, Z. Dong, *ChemSusChem* 11 (2018) 4156–4165, <https://doi.org/10.1002/cssc.201802163>.
- Q. Zhu, X. Sun, H. Zhao, D. Xu, Z. Dong, *Ind. Eng. Chem. Res.* 59 (2020) 5615–5623, <https://doi.org/10.1021/acs.iecr.9b06366>.
- D. Liu, P. Yang, H. Zhang, M. Liu, W. Zhang, D. Xu, J. Gao, *Green Chem.* 21 (2019) 2129–2137, <https://doi.org/10.1039/c8gc03818j>.
- E. Knoevenagel, B. Bergdolt, *Chem. Ber.* 36 (1903) 2857–2860, <https://doi.org/10.1002/cber.19030360334>.
- D. Yadav, S.K. Awasthi, *Green Chem.* 22 (2020) 4295–4303, <https://doi.org/10.1039/d0gc01469a>.
- X. Yan, P. Duan, F. Zhang, H. Li, H. Zhang, M. Zhao, X. Zhang, B. Xu, S. J. Pennycook, J. Guo, *Carbon* 143 (2019) 378–384, <https://doi.org/10.1016/j.carbon.2018.11.021>.
- J. Mao, W. Chen, W. Sun, Z. Chen, J. Pei, D. He, C. Lv, D. Wang, Y. Li, *Angew. Chem. Int. Ed.* 56 (2017) 11971–11975, <https://doi.org/10.1002/anie.201706645>.
- S. Cai, H. Duan, H. Rong, D. Wang, L. Li, W. He, Y. Li, *ACS Catal.* 3 (2013) 608–612, <https://doi.org/10.1021/cs300689w>.
- H. Fu, L. Zhang, Y. Wang, S. Chen, Y. Wan, *J. Catal.* 344 (2016) 313–324, <https://doi.org/10.1016/j.jcat.2016.09.021>.
- S. Zhang, C.R. Chang, Z.Q. Huang, J. Li, Z. Wu, Y. Ma, Z. Zhang, Y. Wang, Y. Qu, *J. Am. Chem. Soc.* 138 (2016) 2629–2637, <https://doi.org/10.1021/jacs.5b11413>.
- L. Shang, T. Bian, B. Zhang, D. Zhang, L. Wu, C. Tung, Y. Yin, T. Zhang, *Angew. Chem. Int. Ed.* 53 (2014) 250–254, <https://doi.org/10.1002/anie.201306863>.
- B.K. Barman, K.K. Nanda, *ACS Sustain. Chem. Eng.* 6 (2018) 12736–12745, <https://doi.org/10.1021/acssuschemeng.8b01861>.
- W.C. Cheong, W. Yang, J. Zhang, Y. Li, D. Zhao, S. Liu, K. Wu, Q. Liu, C. Zhang, D. Wang, Q. Peng, C. Chen, Y. Li, *ACS Appl. Mater. Interfaces* 11 (2019) 33819–33824, <https://doi.org/10.1021/acsami.9b09125>.
- T. Ye, F. Lu, J. Li, T. Nakao, H. Yang, T. Tada, M. Kitano, H. Hosono, *J. Am. Chem. Soc.* 139 (2017) 17089–17097, <https://doi.org/10.1021/jacs.7b08252>.
- Y. Qu, G. Xu, J. Yang, Z. Zhang, *Appl. Catal. A Gen.* 590 (2020), 117311, <https://doi.org/10.1016/j.apcata.2019.117311>.
- Z. Wei, J. Wang, S. Mao, D. Su, H. Jin, Y. Wang, F. Xu, H. Li, Y. Wang, *ACS Catal.* 5 (2015) 4783–4789, <https://doi.org/10.1021/acscatal.5b00737>.
- R.V. Jagadeesh, A.E. Surkus, H. Junge, M.M. Pohl, J. Radnik, J. Rabeah, H. Huan, V. Schunemann, A. Bruckner, M. Beller, *Science* 342 (2013) 1073–1076, <https://doi.org/10.1126/science.1242005>.

- [24] Y. Cao, S. Chen, Q. Luo, H. Yan, Y. Lin, W. Liu, L. Cao, J. Lu, J. Yang, T. Yao, S. Wei, *Angew. Chem. Int. Ed.* 56 (2017) 12191–12196, <https://doi.org/10.1002/anie.201706467>.
- [25] X. Wei, Z. Zhang, M. Zhou, A. Zhang, W.D. Wu, Z. Wu, *Nanoscale* 10 (2018) 16839–16847, <https://doi.org/10.1039/c8nr04775h>.
- [26] L. Liu, P. Concepción, A. Corma, *J. Catal.* 340 (2016) 1–9, <https://doi.org/10.1016/j.jcat.2016.04.006>.
- [27] F. Yang, C. Chi, C. Wang, Y. Wang, Y. Li, *Green Chem.* 18 (2016) 4254–4262, <https://doi.org/10.1039/c6gc00222f>.
- [28] F.A. Westerhaus, R.V. Jagadeesh, G. Wienhofer, M.M. Pohl, J. Radnik, A.E. Surkus, J. Rabeah, K. Junge, H. Junge, M. Nielsen, A. Bruckner, M. Beller, *Nat. Chem.* 5 (2013) 537–543, <https://doi.org/10.1038/nchem.1645>.
- [29] R.V. Jagadeesh, D. Banerjee, P.B. Arockiam, H. Junge, K. Junge, M.M. Pohl, J. Radnik, A. Brückner, M. Beller, *Green Chem.* 17 (2015) 898–902, <https://doi.org/10.1039/c4gc00731j>.
- [30] D. Formenti, F. Ferretti, C. Topf, A.E. Surkus, M.M. Pohl, J. Radnik, M. Schneider, K. Junge, M. Beller, F. Ragaini, *J. Catal.* 351 (2017) 79–89, <https://doi.org/10.1016/j.jcat.2017.04.014>.
- [31] J. Sheng, L. Wang, L. Deng, M. Zhang, H. He, K. Zeng, F. Tang, Y.N. Liu, *ACS Appl. Mater. Interfaces* 10 (2018) 7191–7200, <https://doi.org/10.1021/acscami.8b00573>.
- [32] X. Ma, Y.X. Zhou, H. Liu, Y. Li, H.L. Jiang, *Chem. Commun.* 52 (2016) 7719–7722, <https://doi.org/10.1039/c6cc03149h>.
- [33] P. Zhou, C. Yu, L. Jiang, K. Lv, Z. Zhang, *J. Catal.* 352 (2017) 264–273, <https://doi.org/10.1016/j.jcat.2017.05.026>.
- [34] P. Zhou, Z. Zhang, L. Jiang, C. Yu, K. Lv, J. Sun, S. Wang, *Appl. Catal. B Environ.* 210 (2017) 522–532, <https://doi.org/10.1016/j.apcatb.2017.04.026>.
- [35] H. Li, L. Chi, C. Yang, L. Zhang, F. Yue, J. Wang, *J. Mater. Res.* 31 (2016) 3069–3077, <https://doi.org/10.1557/jmr.2016.314>.
- [36] M. Yuan, H. Zhang, C. Yang, F. Wang, Z. Dong, *ChemCatChem* 11 (2019) 3327–3338, <https://doi.org/10.1002/cctc.201900714>.
- [37] J. Long, Y. Zhou, Y. Li, *Chem. Commun.* 51 (2015) 2331–2334, <https://doi.org/10.1039/c4cc08946d>.
- [38] J. Gonzalez Prior, J.I. Gutierrez Ortiz, R. Lopez Fonseca, G. Busca, E. Finocchio, B. de Rivas, *Catal. Sci. Technol.* 6 (2016) 5618–5630, <https://doi.org/10.1039/c6cy00321d>.
- [39] J. Tian, Q. Liu, C. Ge, Z. Xing, A.M. Asiri, A.O. Al Youbi, X. Sun, *Nanoscale* 5 (2013) 8921–8924, <https://doi.org/10.1039/c3nr02031b>.
- [40] T. Cheng, H. Yu, F. Peng, H. Wang, B. Zhang, D. Su, *Catal. Sci. Technol.* 6 (2016) 1007–1015, <https://doi.org/10.1039/c5cy01349f>.
- [41] X. Sun, A.I. Olivios-Suarez, D. Osadchii, M.J.V. Romero, F. Kapteijn, J. Gascon, *J. Catal.* 357 (2018) 20–28, <https://doi.org/10.1016/j.jcat.2017.10.030>.
- [42] S. Yang, L. Peng, D.T. Sun, E. Oveisi, S. Bulut, W.L. Queen, *ChemSusChem* 11 (2018) 3131–3138, <https://doi.org/10.1002/cssc.201801641>.
- [43] Z. Jiang, W. Lu, Z. Li, K.H. Ho, X. Li, X. Jiao, D. Chen, *J. Mater. Chem. A* 2 (2014) 8603–8606, <https://doi.org/10.1039/c3ta14430e>.
- [44] T. Wang, Z. Dong, W. Cai, Y. Wang, T. Fu, B. Zhao, L. Peng, W. Ding, Y. Chen, *Chem. Commun.* 52 (2016) 10672–10675, <https://doi.org/10.1039/c6cc04713k>.
- [45] D. Mullangi, D. Chakraborty, A. Pradeep, V. Koshti, C.P. Vinod, S. Panja, S. Nair, R. Vaidhyanathan, *Small* 14 (2018), 1801233, <https://doi.org/10.1002/sml.201801233>.
- [46] K. Shen, L. Zhang, X. Chen, L. Liu, D. Zhang, Y. Han, J. Chen, J. Long, R. Luque, Y. Li, B. Chen, *Science* 359 (2018) 206–210, <https://doi.org/10.1126/science.aao3403>.
- [47] T. Schwob, R. Kempe, *Angew. Chem. Int. Ed.* 55 (2016) 15175–15179, <https://doi.org/10.1002/anie.201608321>.
- [48] P. Zhou, L. Jiang, F. Wang, K. Deng, K. Lv, Z. Zhang, *Sci. Adv.* 3 (2017), 1601945, <https://doi.org/10.1126/sciadv.1601945>.
- [49] Z. Zhang, X. Wei, Y. Yao, Z. Chen, A. Zhang, W. Li, W.D. Wu, Z. Wu, X.D. Chen, *D. Zhao, Small* 13 (2017), 1702243, <https://doi.org/10.1002/sml.201702243>.
- [50] D. Xue, D. Zhu, W. Xiong, T. Cao, Z. Wang, Y. Lv, L. Li, M. Liu, L. Gan, *ACS Sustain. Chem. Eng.* 7 (2019) 7024–7034, <https://doi.org/10.1021/acscuschemeng.8b06774>.
- [51] Z. Zhuang, S.A. Giles, J. Zheng, G.R. Jenness, S. Caratzoulas, D.G. Vlachos, Y. Yan, *Nat. Commun.* 7 (2016), 10141, <https://doi.org/10.1038/ncomms10141>.
- [52] C.C. Yang, S.F. Zai, Y.T. Zhou, L. Du, Q. Jiang, *Adv. Funct. Mater.* 29 (2019), 1901949, <https://doi.org/10.1002/adfm.201901949>.
- [53] S. Zhao, J. Yanga, M. Hana, X. Wang, Y. Lin, R. Yang, *Appl. Catal. B Environ.* 260 (2020), 118207, <https://doi.org/10.1016/j.apcatb.2019.118207>.
- [54] W. Zhang, X. Yao, S. Zhou, X. Li, L. Li, Z. Yu, L. Gu, *Small* 14 (2018), 1800423, <https://doi.org/10.1002/sml.201800423>.
- [55] C. Chen, Z. Yang, W. Liang, H. Yan, Y. Tuo, Y. Li, Y. Zhou, J. Zhang, *J. Energy Chem.* 55 (2021) 345–354, <https://doi.org/10.1016/j.jechem.2020.07.017>.
- [56] S. Liu, X. Chen, S. Wang, Z. Yang, J. Gao, P. Zhu, X. Zhao, G. Wang, *Electrochim. Acta* 292 (2018) 707–717, <https://doi.org/10.1016/j.electacta.2018.10.001>.
- [57] C. Zhu, Q. Shi, B.Z. Xu, S. Fu, G. Wan, C. Yang, S. Yao, J. Song, H. Zhou, D. Du, S. P. Beckman, D. Su, Y. Lin, *Adv. Energy Mater.* 8 (2018), 1801956, <https://doi.org/10.1002/aenm.201801956>.
- [58] Y. Qian, Z. Liu, H. Zhang, P. Wu, C. Cai, *ACS Appl. Mater. Interfaces* 8 (2016) 32875–32886, <https://doi.org/10.1021/acscami.6b11927>.
- [59] L. Kong, H. Adidharma, *Chem. Eng. J.* 375 (2019), 122112, <https://doi.org/10.1016/j.cej.2019.122112>.
- [60] L. Yu, H.B. Wu, X.W. Lou, *Acc. Chem. Res.* 50 (2017) 293–301, <https://doi.org/10.1021/acs.accounts.6b00480>.
- [61] S. García Dalí, J.I. Paredes, B. Caridad, S. Villar Rodil, M. Díaz González, C. Fernández Sánchez, A. Adawy, A. Martínez Alonso, J.M.D. Tascón, *Appl. Mater. Today* 20 (2020), 100678, <https://doi.org/10.1016/j.apmt.2020.100678>.
- [62] X. Kong, Z. Sun, M. Chen, C. Chen, Q. Chen, *Energy Environ. Sci.* 6 (2013), 3260, <https://doi.org/10.1039/c3ee40918j>.
- [63] L. Lyu, Y. Kao, D.A. Cullen, B.T. Sneed, Y. Chuang, C. Kuo, *Chem. Mater.* 29 (2017) 5681–5692, <https://doi.org/10.1021/acs.chemmater.7b01550>.
- [64] C. Wang, H. Zhang, C. Feng, S. Gao, N. Shang, Z. Wang, *Catal. Commun.* 72 (2015) 29–32, <https://doi.org/10.1016/j.catcom.2015.09.004>.
- [65] C. Kästner, A.F. Thünemann, *Langmuir* 32 (2016) 7383–7391, <https://doi.org/10.1021/acs.langmuir.6b01477>.
- [66] P. Chen, F. Yang, A. Kostka, W. Xia, *ACS Catal.* 4 (2014) 1478–1486, <https://doi.org/10.1021/cs500173t>.
- [67] L. Zhang, M. Zhou, A. Wang, T. Zhang, *Chem. Rev.* 120 (2020) 683–733, <https://doi.org/10.1021/acs.chemrev.9b00230>.
- [68] L. Zhang, A. Wang, W. Wang, Y. Huang, X. Liu, S. Miao, J. Liu, T. Zhang, *ACS Catal.* 5 (2015) 6563–6572, <https://doi.org/10.1021/acscatal.5b01223>.
- [69] J. Mahmood, S.M. Jung, S.J. Kim, J. Park, J.W. Yoo, J.B. Baek, *Chem. Mater.* 27 (2015) 4860–4864, <https://doi.org/10.1021/acs.chemmater.5b01734>.
- [70] X. Sun, A.I. Olivios Suarez, L. Oar Arteta, E. Rozhko, D. Osadchii, A. Bavykina, F. Kapteijn, J. Gascon, *ChemCatChem* 9 (2017) 1854–1862, <https://doi.org/10.1002/cctc.201700095>.
- [71] Y. Gu, A. Wu, L. Wang, D. Wang, H. Yan, P. Yu, Y. Xie, C. Tian, F. Sun, H. Fu, *J. Mater. Chem. A* 8 (2020) 4807–4815, <https://doi.org/10.1039/c9ta13615k>.
- [72] R. Gao, H. Guo, B. Wang, P. Qiu, M. Sun, L. Chen, *Appl. Catal. A Gen.* 579 (2019) 99–105, <https://doi.org/10.1016/j.apcata.2019.04.024>.
- [73] W. Wu, Q. Zhang, X. Wang, C. Han, X. Shao, Y. Wang, J. Liu, Z. Li, X. Lu, M. Wu, *ACS Catal.* 7 (2017) 7267–7273, <https://doi.org/10.1021/acscatal.7b01671>.
- [74] J.A. Dean, *Lange's Handbook of Chemistry*, 15th ed., McGraw-Hill, New York, 1992.
- [75] B. Chen, F. Li, Z. Huang, G. Yuan, *ChemCatChem* 8 (2016) 1132–1138, <https://doi.org/10.1002/cctc.201501265>.
- [76] H. Zhang, D. Tian, Z. Zhao, X. Liu, Y. Hou, Y. Tang, J. Liang, Z. Zhang, X. Wang, *J. Qiu, Energy Storage Mater.* 21 (2019) 210–218, <https://doi.org/10.1016/j.ensm.2018.12.005>.
- [77] H. Ge, G. Li, J. Shen, W. Ma, X. Meng, L. Xu, *Appl. Catal. B Environ.* 275 (2020), 119104, <https://doi.org/10.1016/j.apcatb.2020.119104>.
- [78] P. Chen, K. Xu, Z. Fang, Y. Tong, J. Wu, X. Lu, X. Peng, H. Ding, C. Wu, Y. Xie, *Angew. Chem. Int. Ed.* 54 (2015) 14710–14714, <https://doi.org/10.1002/anie.201506480>.
- [79] L. Chen, Y. Zhang, X. Liu, L. Long, S. Wang, X. Xu, M. Liu, W. Yang, J. Jia, *Carbon* 151 (2019) 10–17, <https://doi.org/10.1016/j.carbon.2019.05.063>.
- [80] K. Xiao, J. Wang, Z. Chen, Y. Qian, Z. Liu, L. Zhang, X. Chen, J. Liu, X. Fan, Z. X. Shen, *Small* 15 (2019), 1901454, <https://doi.org/10.1002/sml.201901454>.
- [81] H. Sun, C. Tian, G. Fan, J. Qi, Z. Liu, Z. Yan, F. Cheng, J. Chen, C.P. Li, M. Du, *Adv. Funct. Mater.* 30 (2020), 1910596, <https://doi.org/10.1002/adfm.201910596>.
- [82] W. Yuan, S. Wang, Y. Ma, Y. Qiu, Y. An, L. Cheng, *ACS Energy Lett.* 5 (2020) 692–700, <https://doi.org/10.1021/acscenergylett.0c00116>.